CHEMISTRY
A EUROPEAN JOURNAL

FULL PAPER

DOI: 10.1002/chem.201301806

Reversible Pore Size Control of Elastic Microporous Material by Mechanical Force

Masashi Ito,[a, b] Hirotomo Nishihara,*[a] Kentaro Yamamoto,[a] Hiroyuki Itoi,[a] Hideki Tanaka,[c] Akira Maki,[c] Minoru T. Miyahara,[c] Seung Jae Yang,[d] Chong Rae Park,[d] and Takashi Kyotani[a]

Abstract: Nanoporous materials, such as zeolites, activated carbons, and metal–organic frameworks (MOFs), are peculiar platforms in which a variety of guest molecules are stored, reacted, and/or separated. The size of the nanopores is essential to realize advanced functions. In this work, we demonstrate a very simple but innovative method for the control of nanopore size, that is, reversible and continuous control by mechanical force loaded to soft nanoporous materials. The elastic properties of several microporous materials, including zeolites, zeolite-templated carbon (ZTC), activated carbon, and MOFs (e.g., ZIF-8), are examined and it is found that ZTC is a material that is suitable for the aforementioned idea thanks to its extraordinary soft properties compared to the others. The original pore size of ZTC (1.2 nm) can be contracted to 0.85 nm by using a relatively weak loading force of 135 MPa, whereas the other microporous materials barely contracted. To demonstrate the change in the physical properties induced by such artificial deformation, in situ gas adsorption measurements were performed on ZTC with and without loading mechanical force, by using CO_2, CH_4, and H_2, as adsorbates. Upon the contraction by loading 69 or 135 MPa, CO_2 adsorption amount is increased, due to the deepening of the physisorption potential well inside the micropores, as proved by the increase of the heat of adsorption. Moreover, the adsorption amount is completely restored to the original one after releasing the mechanical force, indicating the fully reversible contraction/recovery of the ZTC framework against mechanical force. The experimental results are theoretically supported by a simulation using Grand Canonical Monte Carlo method. The similar adsorption enhancement is observed also on CH_4, whereas H_2 is found as an exception due to the weak interaction potential.

Keywords: graphene · metal–organic frameworks · nanomaterials · physisorption · zeolites

Introduction

Nanoporous materials, such as zeolites,[1–3] mesoporous silicas,[4–6] metal–organic frameworks (MOFs),[7–9] and nanoporous carbons[10–14] have been widely used as adsorbents, separation media, catalysts/catalyst supports, and electrodes. In such applications, pore-size control is important because the pore size governs the physical properties and functions of the nanoporous materials, that is, adsorption capability, diffusion rate, and molecular sieving. Conventionally, pore-size control has been achieved, in many cases, by preparing nanoporous materials with specific target pore sizes. For example, various types of crystalline microporous materials, such as zeolites and MOFs, have been intensively synthesized through a variety of techniques, to realize different topology, dimension, and sizes of their micropores.[2,7,8] As is found in zeolites, for which these are more than 200 types of different crystal structures, pore-size effects on adsorption/sieving functions are of significance at the level of Ångström to sub-Ångström. In mesoporous materials, similar strategies have been commonly used to tailor pore sizes, for example, a variety of mesoporous silicas, mesoporous carbons, or other mesoporous materials.[12,13,15,16] Pore size can also be controlled by post-synthesis modification. For example, it is

[a] M. Ito, Prof. H. Nishihara, K. Yamamoto, Dr. H. Itoi, Prof. T. Kyotani
Institute of Multidisciplinary Research for Advanced Materials
Tohoku University, 2-1-1, Katahira
Aoba-ku, Sendai, 980-8577 (Japan)
Fax: (+81) 22-217-5626
E-mail: nisihara@tagen.tohoku.ac.jp

[b] M. Ito
Advanced Materials Laboratory
Nissan Research Center, Nissan Motor Co., Ltd.
1,Natsushima-cho, Yokosuka-shi Kanagawa 237-8523 (Japan)
Fax: (+81) 46-866-5336

[c] Dr. H. Tanaka, A. Maki, Prof. M. T. Miyahara
H. Tanaka, A. Maki, M. T. Miyahara
Department of Chemical Engineering, Kyoto University
Katsura, Nishikyo, Kyoto 615-8510 (Japan)

[d] Dr. S. J. Yang, Prof. C. R. Park
Carbon Nanomaterials Design Laboratory
Global Research Laboratory
Research Institute of Advanced Materials, and
Department of Materials Science and Engineering
Seoul National University, Seoul 151-744 (Republic of Korea)

Supporting information for this article is available on the WWW under http://dx.doi.org/10.1002/chem.201301806.

possible to reduce pore sizes of zeolites, mesoporous silicas, and activated carbons, through a chemical vapor deposition or chemical modifications,[17–19] while enlargement of pore size in anodic aluminum oxide[20] can be achieved by chemical etching.

There is actually another methodology for varying pore size: reversible pore-size change induced by the inclusion/exclusion of guest molecules. Some of MOFs that originally have narrow pores can be expanded by the inclusion of guest molecules.[21–24] Similar pore expansion can be seen in some nanoporous materials with soft frameworks, such as nanoporous poly(imide),[25] and a specific templated carbon.[26] However, these methods cannot be used to control the size of "empty" nanopores. If it is possible to freely deform "empty" nanopores by an external stimulus without the help of guest molecules, the absorption ability (or properties) of a porous material itself could be altered intentionally. Such an epochal technology would give rise to a significant advance in the fields of adsorption science and nanopore engineering.

In this work, we propose a very simple but innovative methodology for nanopore-size control; continuous and reversible control by mechanical force loaded to soft nanoporous materials. Figure 1 illustrates this idea. By loading mechanical force to a nanoporous material, the nanopores are contracted, and the physisorption potential is increased, which is expected to give rise to the enhancement of molecular adsorption (from Figure 1a to 1b).[27] Further contraction results in prohibiting the adsorption due to a sieving effect (from Figure 1b to 1c). When the applied force is gradually released, the nanopores and the corresponding adsorption amount are recovered up to the original state (from Figure 1c, 1b, and to 1a).

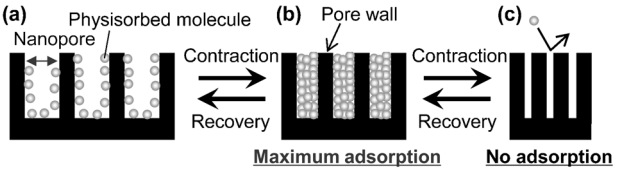

Figure 1. Illustration for the continuous and reversible pore-size control by loading mechanical force, and the resulting change in molecular physisorption amount.

Such pressure-induced reversible and continuous deformation of nanopores has actually been reported on a mesoporous silica.[28] However, a robust silica framework is only slightly contracted (ca. 5%) even by a very high pressure of 12 GPa. In addition, Cazorla et al. observed elastic deformation of micropores in activated carbon fibers by micro small-angle X-ray scattering, however, the maximum strain was only 2.8% by a tensile stress of 600 MPa.[29] To realize the idea shown in Figure 1, nanoporous materials consisting of much more flexible frameworks have to be used. In addition, the nanopore size should be uniform to clearly detect the size change and the corresponding impact on the physical properties. Herein, we demonstrate that a part of the hypothetical idea shown in Figure 1 is actually realized with a zeolite-templated carbon (ZTC), an ordered microporous carbon synthesized using a zeolite template.[30,31] We have previously reported that hot-pressing of ZTC at 573 K enables irreversible decrease of its pore size.[32] Similar "pressure-induced pore-size control" has been reported also for MOFs.[33] In these cases, however, their frameworks gradually collapse and the structure changes are therefore irreversible, due to very severe pressing conditions, that is, high temperature and/or pressure. Another example is a very flexible MOF, MIL-53(Cr),[34] which shows a reversible structural transition between pore opening and closing induced by the change in hydrostatic pressure. However, the continuous deformation of the pore size is not possible in this case. Thus, these methods are essentially different from the present strategy shown in Figure 1 aiming at reversible and continuous pore-size control within the limited pressure range in which a nanoporous material shows elastic deformation. We demonstrate here that ZTC is remarkably flexible compared with other microporous materials (zeolite, activated carbon, and MOF), and that the gas sorption behavior of ZTC could be altered by its reversible compression/restoration induced by mechanical force.

Results and Discussion

Structures and morphologies of microporous materials: In this work, ZTC and two reference microporous materials were investigated. Molecular-level structures of these materials are shown in Figure 2, together with their scanning electron microscope (SEM) images. The details of these materials are as follows:

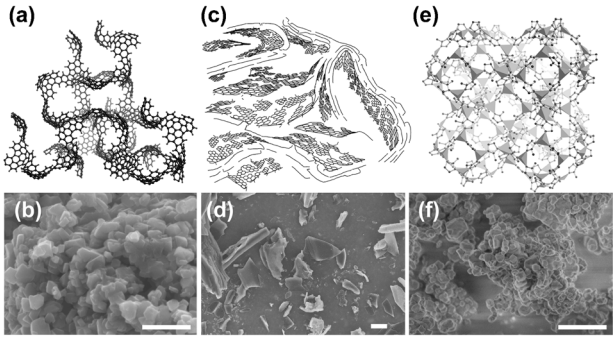

Figure 2. Illustrations of molecular-level structures (a, c, e) and SEM images (b, d, f) of microporous materials used in this work: a) and b) ZTC, c) and d) AC, and e) and f) ZIF-8. Scale bars in SEM images are 1 μm for b) and f) and 10 μm for d).

ZTC: ZTC (Figure 2a) was synthesized by using zeolite Y as a hard template, according to the method reported elsewhere.[35] This carbon, a negative replica of the zeolite template, has ordered micropores the

size of which is very uniform (1.2 nm). The framework is comprised of buckybowl-like curved nanographenes crosslinking each other as shown in Figure 2a. ZTC takes over crystalline powder form derived from the zeolite template with a particle size of about 200 nm, as shown in Figure 2b.

AC: An activated carbon (AC; Shirasagi P, Japan Enviro-Chemicals, Ltd.) was used as one of the reference microporous materials. The present AC was prepared by steam activation and its framework is composed of randomly arranged defective graphene sheets as illustrated in Figure 2c. As shown in Figure 2d, this carbon is a powder form with sizes of 1–20 μm.

ZIF-8: The second reference microporous material was one of the MOFs, ZIF-8[36] (Basolite® Z1200, Sigma Aldirich Inc.). It is classified as a zeolitic imidazolate framework, and its structure is shown in Figure 2e, in which tetrahedrally-coordinated Zn^{2+} ions are connected by imidazole linkers. Thus, ZIF-8 has a zeolite-like ordered framework forming uniform spherical micropores with a diameter of 1.2 nm. ZIF-8 is crystalline powder like zeolite crystal with average diameter of 150 nm, as shown in Figure 2f.

Mechanical properties of microporous materials: First, the mechanical properties of powder samples were examined by using mercury as a mediator of force for measuring stress–strain curves under isotropic pressure. As generally known in mercury porosimetry, mercury cannot invade into micropores (<2 nm) even under pressure, and it is thus possible to characterize the mechanical properties of the powder samples by using a mercury porosimeter. The measurement results are shown in Figure 3, in which V_{Hg} and V_0 are a volume change of mercury and an initial sample volume (including micropore volumes), respectively. In Figure 3, zeolite Y shows a rapid increase in V_{Hg}/V_0 at very low pressure, corresponding to Hg impregnation into interparticle spaces.

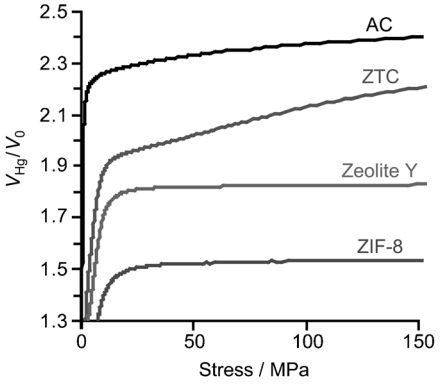

Figure 3. V_{Hg}/V_0 versus stress loaded to Hg in microporous powders measured by the mercury porosimeter. V_{Hg} and V_0 are the volume change of mercury and initial sample volume (including micropore volumes), respectively.

Such a rapid increase is almost saturated below 20 MPa, and at higher pressure, the stress–strain curve becomes linear, corresponding to the contraction of the zeolite particles. As shown in Figure 2b, ZTC is a negative replica of zeolite Y, and thus the particle morphology of ZTC is the same as that of zeolite Y. A rapid increase in V_{Hg}/V_0 at low pressure is therefore saturated below 20 MPa also in ZTC, and a linear part above 20 MPa is ascribed to the contraction of the ZTC particles. Since the particle morphology of ZIF-8 is close to that in ZTC (Figure 2b and f), the interpretation of the stress–strain curves for zeolite Y and ZTC can be also applied to ZIF-8. All of zeolite Y, ZTC, and ZIF-8 are purely microporous materials, and therefore it is easy to separate the contributions of the Hg impregnation into interparticles from the contraction of each particle in Figure 3. However, it is not straightforward in AC, because AC could have larger mesopores and/or macropores, as we will show later.

Next, the compressibility (β) of the microporous particle was calculated from Figure 3, and bulk modulus (κ) was obtained as a reciprocal of β. Table 1 summarizes β and κ determined by taking a slope on each of the stress–strain curves at 60–150 MPa. The bulk modulus of zeolite Y is 13 GPa, a little lower than those found in the literatures,[37,38] probably due to the low pressure range in this work. ZIF-8 showed lower bulk modulus (9.2 GPa) than that of zeolite Y, indicating the soft property of ZIF-8, as Tan et al. has reported.[37] Though AC shows low bulk modulus, such a value must be underestimated, due to the presence of meso- and macropores. It is worth noting that ZTC shows remarkably low bulk modulus (0.51 GPa), indicating its extraordinary flexibility. The bulk modulus of ZTC is indeed lower than those of polymers such as polystyrene (4 GPa) and polymethyl methacrylate (6 GPa).[39] This exceptional flexibility of ZTC is due to its nanographene-based framework shown in Figure 2a. It is known that nanocarbons, such as single-walled carbon nanotubes[40] and graphenes,[41,42] show significant flexibility, while graphite is a hard solid, although all of them intrinsically consist of a graphene sheet(s), that is, a two-dimensional crystal composed of sp^2 C–C bonds. Thus, mechanical properties of graphene-based architectures highly depend on their morphologies as well as their arrangements, that is, stacking, aggregating, and/or network structures. The unique framework structure shown in Figure 2a makes ZTC as an extraordinary "soft" microporous material. Consequently, it is expected that the pore size of

Table 1. Mechanical properties of microporous materials below 150 MPa.

Sample	Compressibility[a] [Pa^{-1}]	Bulk modulus[b] [GPa]
ZTC	2.0×10^{-9}	0.51
AC	6.5×10^{-10}	1.5
ZIF-8	1.1×10^{-10}	9.2
Zeolite Y	7.7×10^{-11}	13

[a] Obtained from a stress–strain curve (at 60–150 MPa) measured with mercury as a mediator of force. [b] Bulk modulus is calculated as a reciprocal of the compressibility.

ZTC can be reversibly controlled at a detectable level, simply by loading a mechanical force.

In situ measurement of CO_2 adsorption isotherm under loading mechanical force: One of the purposes of this work is the in situ measurement of gas adsorption isotherm on ZTC under loading mechanical force. An experimental setup for the in situ measurement is illustrated in Figure 4.

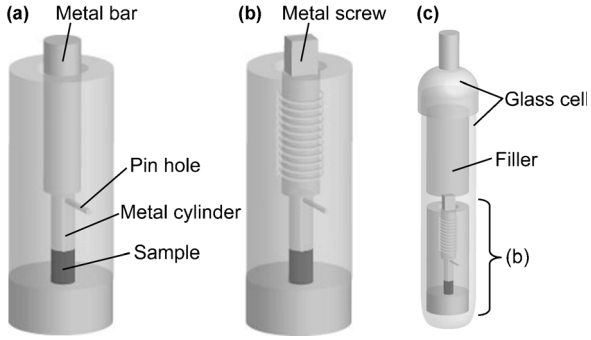

Figure 4. An experimental setup for the measurement of gas adsorption isotherms under loading mechanical force to the samples. a) A set of molds made from cemented carbide for stabilizing the packing state of the sample bed as well as for measurements of stress–displacement curves of the sample bed. A sample placed inside the mold is connected to outside through a pin hole, which is the path for the gases. b) A set of mold for gas adsorption measurements. The metal bar in the setup shown in a) is replaced with a metal screw by which a constant force can be loaded to the sample bed. c) A glass cell including the whole experimental set-up shown in b) and a metal filler, which is for decreasing a dead volume. The glass cell is connected to a gas adsorption/desorption analyzer, and isotherms of CO_2, CH_4, and H_2 were measured.

First, a powder sample was placed in a cemented-carbide mold as shown in Figure 4a, and a pressing–releasing cycle was repeated ten times to stabilize the packing of the particles. The stress–displacement curves of ZTC during such cycles are shown in Figure 5a, as an example. Note that the deformation of the metal mold itself is very small, but it was measured by a blank experiment and was subtracted in all the experiments shown hereafter. At the first run, large displacement is observed due to the significant relocation of each particle, and the sample bed is irreversibly compressed, as is found from the upward shift of the starting point (4.4 mm at 0 MPa) in the second run. By repeating the contraction–recovery cycles, the packing of the sample bed is gradually stabilized, and the results of ninth and tenth compressions are almost the same, indicating that the sample bed is fully stabilized by the tenth cycle.

The sample beds of AC and ZIF-8 were also compressed and fully stabilized by the tenth cycle in the same manner as described above. For each sample, after the tenth cycle, a metal bar (Figure 4a) was replaced with a metal screw, which has exactly the same length as that of the metal bar, as shown in Figure 4b, and then mechanical force was again loaded to the sample bed with the screw. Note that it is possible to precisely determine the pressure loaded to the

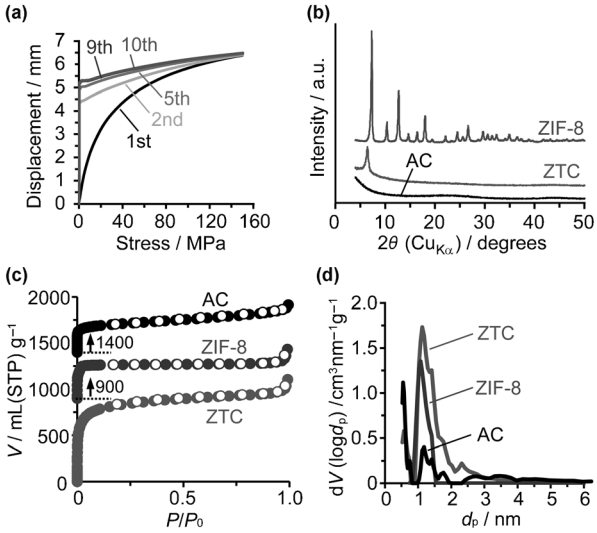

Figure 5. a) Stress-displacement curves of ZTC powder during the pressing–releasing cycles. The origin of the displacement (0 mm) corresponds to the original height of the sample bed before any compression. The pressing–releasing cycle is repeated ten times, and the results at 1st, 2nd, 5th, 9th, and 10th cycle are shown here. b) XRD patterns, c) N_2 adsorption–desorption isotherms (77 K), and d) pore-size distributions (DFT method) of the sample beds after ten pressing–releasing cycles. In c), the isotherms of ZIF-8 and AC are shifted upward by 900 and 1400 mL(STP) g^{-1}, respectively, for a clearer view.

sample bed by the screw, based on the stress–displacement curve of the tenth cycle in each of samples. In this work, the stress was adjusted at 69 or 135 MPa. Then, the cemented-carbide mold including the sample (Figure 4b) was put into a glass vessel that is connected to an automatic adsorption analyzer to carry out the in situ measurements of gas adsorption isotherms under loading mechanical pressure to the sample (Figure 4c).

The textural properties of the compressed samples were characterized by X-ray diffraction (XRD) and N_2 cryosorption (77 K) beforehand, in the separate experiments. Figure 5b shows XRD patterns of the sample beds after ten pressing–releasing cycles up to 150 MPa. Even after the repeated compression, ZTC shows its characteristic peak at $2\theta = 6.4°$, corresponding to its ordered framework structure shown in Figure 2a. ZIF-8 also shows characteristic peaks (Figure 5b) derived from its crystal structure.[36] Unlike ZTC and ZIF-8, AC has disordered structure represented in Figure 2c, and therefore it does not show any sharp peak: AC only shows a broad and weak carbon (002) peak around $2\theta = 24°$. The XRD patterns of these three materials clearly reflect the individual nanostructures illustrated in Figure 2. N_2 adsorption–desorption isotherms (77 K) of these samples are shown in Figure 5c. Their isotherms are close to type I, so that they are basically microporous materials. The BET surface areas (S_{BET}), pore volumes (V_{micro} and V_{total}), and pore size of the three materials calculated from Figure 5c are summarized in Table 2. The ratios of micropore volume ($V_{micro}/V_{total} \times 100$) in AC, ZIF-8, and ZTC are 63, 92, 89%, respectively. Thus, AC is actually found to have a noticeable

Table 2. Surface areas, pore volumes, pore sizes of the microporous materials obtained from Figure 5c and 5d.

Sample	S_{BET}[a] [m^2g^{-1}]	V_{micro}[b] [cm^3g^{-1}]	V_{total}[c] [cm^3g^{-1}]	Pore size[d] [nm]
AC	1140	0.45	0.71	0.55
ZIF-8	1490	0.58	0.63	1.2
ZTC	3140	1.35	1.51	1.2

[a] BET surface area calculated at $P/P_0=0.01$–0.05. [b] Micropore volume calculated by the Dubinin–Radushkevich method. [c] Total pore volume estimated from the adsorption amount of N_2 at $P/P_0=0.96$. [d] The peak pore size in Figure 5d.

fraction of larger pores (>2 nm), and this accords to the result of Hg intrusion on AC in Figure 3, in which Hg impregnation into macro/mesopores was suggested. Pore size distributions (DFT method) of the sample beds are shown in Figure 5d. As is expected from their structures (Figure 2a and e), ZTC and ZIF-8 have a sharp peak at 1.2 nm, whereas AC shows relatively a distributed pattern.

The in situ CO_2 isotherms of ZTC, AC, and ZIF-8 are shown in Figure 6a, b, and c, respectively. In Figure 6a, the

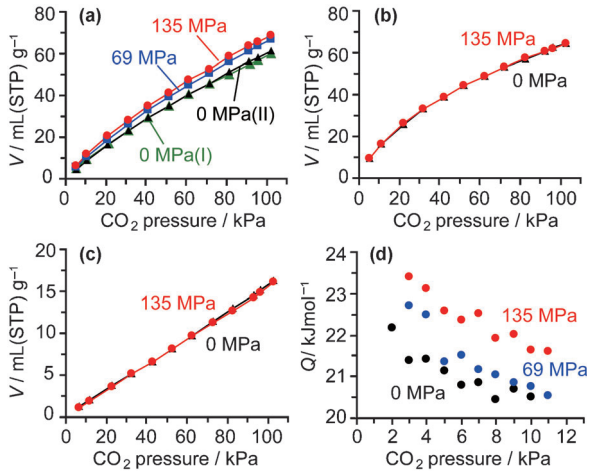

Figure 6. a) CO_2 adsorption isotherms of ZTC at 298 K with and without loading mechanical force: before loading force (0 MPa(I)), loading 69 MPa, 135 MPa, and after recovered to 0 MPa (0 MPa(II)). b) and c) CO_2 adsorption isotherms of b) AC and c) ZIF-8 at 298 K with and without loading 135 MPa. d) The effect of mechanical force on the isosteric heat of sorption (Q) of CO_2 on ZTC.

CO_2 adsorption amount is apparently increased upon loading mechanical force to ZTC. This is ascribed to the increase of physisorption potential by the decrease of pore size.[27] In addition, after releasing the mechanical pressure (after setting the screw to the original position), adsorption amount of CO_2 is recovered as that of the original one, clearly indicating that the deformation of ZTC is fully reversible owing to its extraordinary flexible framework consisting of nanographene network. Although the presently observed phenomenon, that is, the increase of gas adsorption amount by loading mechanical force, is based on a very simple and understandable mechanism as shown in Figure 1, we emphasize that this is actually the first report in which experimental data are indeed shown systematically. The uniqueness of the data shown in Figure 6a can be better understood by the comparative experiment on AC and ZIF-8, shown in Figure 6b and c, respectively. These microporous materials, including the "soft" ZIF-8, show completely no change even by loading 135 MPa, indicating that the nanopores of these materials are not contracted at all. To further confirm the mechanism of the adsorption enhancement, the same protocol in Figure 6a was repeated also at 273 K, and the isosteric heat of sorption (Q) was calculated, according to the Clausius–Clapeyron equation.[35] As shown in Figure 6d, Q is indeed increased by loading mechanical force, and this is the direct evidence of the increase in the physisorption potential by the mechanism explained in Figure 1.

From the tenth stress–displacement curve in Figure 5a, compressibility (β_{uni}) and bulk modulus (κ_{uni}) under unidirectional pressing with the restriction of deformation toward vertical direction can be defined independently from β and κ. ZTC shows very large β_{uni} of 2.1×10^{-9} Pa^{-1}, thereby very small κ_{uni} of 0.47 GPa, again indicating its extraordinary flexible mechanical property also for the unidirectional deformation. By using κ_{uni}, the pore sizes under pressure at 69 and 135 MPa can be estimated to be 1.0 and 0.85 nm, respectively. The pore-size change in ZTC is at the level of Ångström, but it is large enough to change the physisorption behavior for CO_2 (3.3 Å)[43] at a detectable level. We will further examine the physisorption behavior of H_2 (2.89 Å) and CH_4 (3.8 Å)[43] in a later section.

Simulation of CO_2 adsorption isotherms: To evaluate the results shown in Figure 6a, CO_2 adsorption isotherms on ZTC under pressure were theoretically calculated. Starting from the average structure model of ZTC[31] (Figure 2a), compressed models as well as the pristine model were constructed simply by contracting the average model only to the ⟨001⟩ direction, followed by the structure relaxation using the Monte Carlo (MC) simulation (constant NVT) with reaction state summation (RSS) potential.[44–46] The volume fractions of the models thus prepared are 100 (corresponding to the pristine structure), 88, and 71%. The last two models have comparable volume fractions to those calculated by β_{uni} (85% at 69 MPa and 71% at 135 MPa). Adsorption isotherms of the pristine ZTC and the compressed ZTCs were calculated with the Grand Canonical Monte Carlo (GCMC) method. We have confirmed that the pore-size distribution of the ZTC structure shifts to smaller range with keeping its original narrow width (Supporting Information). Figure 7 shows the simulated isotherms together with snapshots at 101.3 kPa of CO_2 pressure for each of the ZTC structures with different degrees of contraction. The simulated isotherm on the pristine structure (Figure 7a) agrees well with the one obtained by the experiment (Figure 6a, 0 MPa): the CO_2 uptake at 100 kPa is 60.2 and 61.5 mL(STP) g^{-1} in experiment and simulation, respectively. In ad-

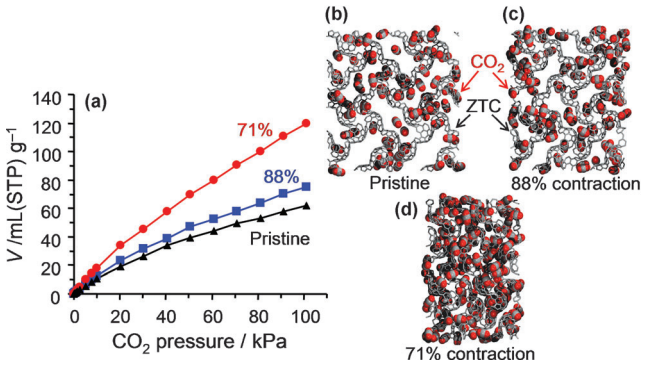

Figure 7. a) CO_2 isotherms on the average structure model of ZTC (Pristine) and the structures with 88% and 71% compression at 298 K. (b-d) Snapshots at 101.3 kPa of CO_2 pressure in the structure models of b) pristine ZTC, c) 88% compression, and d) 71% compression.

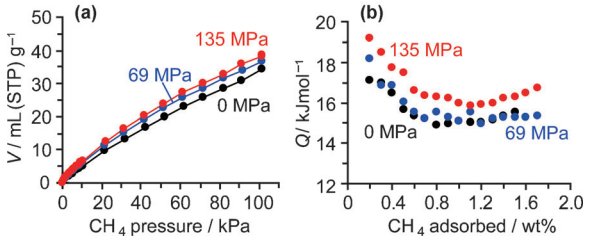

Figure 8. a) CH_4 isotherms on ZTC before loading mechanical force (0 MPa) and under loading 69 and 135 MPa at 273 K. b) The effect of mechanical force on Q of CH_4 on ZTC.

dition, the simulation results basically show the same tendency in the change of the CO_2 adsorption amount upon the contraction of ZTC. The CO_2 adsorption amount is apparently increased by the contraction of the framework. This is due to the increase in the physisorption potential, induced by the pore narrowing. The qualitative agreement between the experiment and simulation strongly supports successful demonstration of our idea shown in Figure 1 in the present work. It should, however, be noted that the simulated CO_2 adsorption amount on the compressed ZTCs (Figure 7a) is much larger than the experimental results shown in Figure 6a. This could be underestimation of the CO_2 adsorption amount in the experiment due to diffusion resistance in the sample bed. When ZTC is compressed under 135 MPa, the ZTC powder is molded into a continuous pellet 5 mm in diameter and 2.8 mm in thickness. As shown in Figure 4b, the compressed sample bed having the continuous pellet form is mostly surrounded by the metal mold, and the sample bed is connected to outside through a pin hole (the path of gas). Note that only about 1.5% of the surface of the ZTC pellet (total surface is 0.83 cm^2) is actually exposed to gas phase, in order to avoid a loss of the powdery sample from the exposed part. Therefore, the diffusion resistance inside the ZTC pellet inevitably becomes large, and this could result in lower adsorption amount in the experiment (Figure 6a) than the equilibrium amount estimated by the simulation (Figure 7a). The simulation results thus suggest that further increase of the in situ adsorption amount by improving the diffusion problem during the pressing. In Figure 7a, the amount of CO_2 sorption reaches 119 $mL\,g^{-1}$ at 100 kPa on the 71%-compressed structure. This amount is about 1.7 times higher than the sorption amount on the pristine ZTC structure. Such remarkable increase would offer new technologies, for example, gas sensing and gas storage based on the physical deformation of micropores.

In situ measurement of CH_4 and H_2 adsorption isotherms on ZTC under loading mechanical force: As demonstrated above, we have successfully shown the increase in the gas physisorption amount experimentally for the first time. From its very simple mechanism, it is expected that the present methodology could be universally adopted for other gases. Thus, we performed the in situ gas sorption measurements also using CH_4 and H_2, under loading pressure on ZTC. Figure 8a shows CH_4 adsorption isotherms on ZTC with and without loading mechanical force (69 and 135 MPa) at 273 K. As was expected, the CH_4 adsorption amount was increased by loading mechanical force on ZTC like the case of CO_2 adsorption (Figure 6a). In addition, the dependence of Q of CH_4 on the mechanical force is also similar to that in CO_2 (Figure 6d). Though Q at 135 MPa shows slight increase above 1.0 wt% of CH_4 uptake, it might be artifact due to experimental error. Thus, the methodology shown in Figure 1 is found to be commonly adapted both on CO_2 and CH_4 adsorption, suggesting a wide range of applicability of this technique. However, there is an exceptional case: it was found in hydrogen adsorption at 273 K that the adsorption amount was not changed by loading mechanical force on ZTC (see the Supporting Information, Figure S2). The reason could be the difference in the profile of the physisorption potential among CO_2, CH_4, and H_2. The interaction between H_2 and a carbon surface is much weaker than those in CO_2 or CH_4, as is found from their Q values on ZTC: CO_2 (20–22 $kJ\,mol^{-1}$, in Figure 6d), CH_4 (14–17 $kJ\,mol^{-1}$, in Figure 8b), and H_2 (6–8 $kJ\,mol^{-1}$).[35] Since the potential well in H_2 physisorption is shallow due to the weak interaction, a small degree of the pore narrowing is not effective to deepen the synthetic potential well that is formed inside a nanopore (see the Supporting Information, Figure S3).

Conclusion

The bulk modulus of ZTC is remarkably low (0.51 GPa), compared to other microporous materials, such as AC (1.5 GPa), ZIF-8 (9.2 GPa), and zeolite Y (13 GPa), at a low-pressure region below 150 MPa. The bulk modulus of ZTC is even lower than those of polystyrene and epoxy resin. Such extraordinary flexibility of ZTC is ascribed to its nanographene-based porous framework. Due to the soft framework, ZTC can be contracted to 71% of its original volume by loading a relatively weak force such as 135 MPa, whereas other microporous materials are barely contracted.

Thus, its initial pore size (1.2 nm) is also remarkably contracted unlike others. To demonstrate the change of physical property induced by the artificial deformation of the microporous framework, in situ gas adsorption measurement is performed on ZTC with and without loading mechanical force, by using CO_2, CH_4, and H_2, as adsorbates. Upon the contraction by loading 69 or 135 MPa, CO_2 adsorption amount is increased, due to the deepening of the physisorption potential well inside the micropores, as proved by the increase in the heat of adsorption. Moreover, the adsorption amount is completely restored to the original one after releasing the mechanical force, indicating the fully reversible contraction/recovery of the ZTC framework against mechanical force. Such a change in adsorption is not observed in other microporous materials under the same experimental conditions, although ZIF-8 is known as a "soft" material. To the best of our knowledge, this is the first report demonstrating experimentally the change in the adsorption amount induced by mechanical force. Moreover, the experimental results are theoretically supported by a simulation using the Grand Canonical Monte Carlo method. In addition, the simulation suggests a restriction of adsorption amount in the present experimental system due to diffusion resistance, which implies that further enhancement is possible by the present approach. The similar adsorption enhancement is observed also on CH_4, indicating a wide applicability of the present method to a variety of host molecules. However, physisorption of H_2 at 273 K is found as an exception due to the weak interaction potential. The present approach, that is, reversible contraction/recovery by mechanical force, is very simple but allows the control of nanopore size at an accuracy at the Ångström level, thereby inducing detectable change in the physical property of the nanoporous materials. This work has demonstrated that this new methodology can work on ZTC, a very flexible microporous material. However, if similar soft porous materials are developed in future, for example, from metal–organic frameworks[7–9] or porous organic frameworks,[47] the present methodology will be applicable also to such soft porous materials.

Experimental Section

Microporous materials: ZTC was synthesized by the method reported elsewhere.[35] A composite of polyfurfuryl alcohol and zeolite Y (Tosoh, HSZ-320NAA) was gradually heated to 973 K under N_2 flow. Subsequently, a chemical vapor deposition of propylene (7% vol in N_2) was performed for 2 h at 973 K, followed by a heat-treatment at 1173 K for 3 h under N_2 flow. Then the zeolite template was dissolved away by HF etching to obtain ZTC. AC (Shirasagi P) was kindly provided from Japan EnviroChemicals, Ltd. ZIF-8 (Basolite® Z1200) was purchased from Sigma Aldirich Inc.

Characterization: The microporous materials were observed by using SEM (Hitachi, S-4800). Mechanical properties of the microporous materials were characterized from stress–strain curves obtained by mercury intrusion porosimetry using an Autopore IV 9510 instrument (Micromeritics Instrument Corporation, Norcross, GA, USA). The sample powder was first placed in a closed chamber, and mercury was introduced into the chamber under vacuum. Pressure was then loaded to mercury with measuring its volume change (V_{Hg}). Note that V_{Hg} consists of a volume decrease due to Hg impregnation into inter-particle spaces (V_{pore}) of powder and a volume decrease due to contraction of microporous particles (V_{cont}). Accordingly, they are related by Equation (1) On the other hand, a volume occupied by the microporous particles (V_0) was calculated by Equation () in which m and $\rho_{particle}$ are a sample weight and a particle density of the microporous material, respectively. This last parameter can be calculated from Equation (3) using a true density (ρ_{true}) and a total pore volume (V_{total}).

$$V_{Hg} = V_{pore} + V_{cont} \tag{1}$$

$$V_0 = \frac{m}{\rho_{particle}} \tag{2}$$

$$\rho_{particle} = \{1/\rho_{true} + V_{total}\}^{-1} \tag{3}$$

For each sample, ρ_{true} and V_{total} were determined by He pycnometry and nitrogen cryosorption at 77 K, respectively. In Figure 3, each sample shows rapid increase in V_{Hg}/V_0 at very low pressure. This is due to a significant contribution of V_{pore}. At higher pressure, Equation (4) can be assumed. The compressibility (β) is calculated from Equation (5).

$$\Delta V_{Hg} = \Delta V_{cont} \tag{4}$$

$$\beta = -\frac{1}{V_0}\frac{\Delta V_{cont}}{\Delta P} \tag{5}$$

For the in situ gas sorption measurements, the powder sample was first put into the cemented-carbide mold shown in Figure 4a, and a pressing–releasing cycle was repeated ten times to stabilize the packing of the particles. The stress–displacement curves during this process were recorded by using Autograph (AG-50kNXDplus, Shimazu Co.). A metal bar (diameter is 8 mm, Figure 4a) was then replaced with a metal screw, which had exactly the same length as that of the metal bar, as shown in Figure 4b, and mechanical force was loaded to the sample bed with the screw. From the displacement of the screw, the pressure loaded to the sample bed was calculated based on the tenth stress–displacement curve. The cemented-carbide mold including the sample (Figure 4b) was put into a glass vessel that is connected to an automatic adsorption analyzer (BEL Japan, BELSORP-max) to carry out the in situ measurements of gas adsorption isotherms under loading mechanical pressure to the sample (Figure 4c). CO_2, CH_4, and H_2 were used as adsorbates.

The ordered structure and textural properties of the sample beds before the in situ gas sorption measurements were characterized by XRD measurements with an X-ray diffractometer (Shimadzu, XRD-6100) with $Cu_{K\alpha}$ radiation generated at 30 kV and 20 mA and nitrogen physisorption measurements at 77 K on the automatic adsorption analyzer and, respectively. The specific surface areas were calculated by the Brunauer–Emmett–Teller (BET) method, using the data at the relative pressure range of 0.01–0.05. The micropore volumes were calculated from the Dubinin–Radushkevich (DR) equation. Total pore volumes (V_{total}) were calculated from the adsorbed amount at P/P_0 is 0.96. Pore size distribution was calculated by the density functional theory (DFT).

Simulation: The average structure model of ZTC consisting of $2\times2\times2$ unit cells (lattice constant of a unit cell: 2.407 nm) was used for the simulation. The structure change of the ZTC model upon the contraction to its $\langle001\rangle$ direction was simulated by using the Monte Carlo (MC) method with reaction state summation (RSS) potential.[44–46] Adsorption isotherms of the pristine ZTC and the compressed ZTC were calculated with the Grand Canonical Monte Carlo (GCMC) method. For the intermolecular interactions of the classical CO_2, N_2, and CH_4 molecules, the Lennard–Jones (LJ) potential was used. The Feynman–Hibbs effective potential based on the LJ potential was used for the intermolecular interaction of H_2 to take into account quantum effects at a low temperature.[47] The LJ interaction parameters are as follows; 1) CO_2: three-center model, $\sigma_{ff,O}=3.033$ Å, $\varepsilon_{ff,O}/k=80.507$ K, $\sigma_{ff,C}=2.757$ Å, $\varepsilon_{ff,C}/k=28.129$ K, bond length $l_{C-O}=1.18$ Å, 2) N_2: two-center model, $\sigma_{ff}=3.32$ Å, $\varepsilon_{ff}/k=36.4$ K, $l_{N-N}=1.1$ Å, 3) H_2: one-center model, $\sigma_{ff}=2.96$ Å, $\varepsilon_{ff}/k=$

34.2 K, 4) CH_4: one-center model, $\sigma_{ff}=3.817$ Å, $\varepsilon_{ff}/k=148.2$ K, and 5) carbon atoms in ZTC: $\sigma_{ss}=3.43$ Å, $\varepsilon_{ss}/k=52.86$ K. All the solid-fluid cross interaction parameters were obtained by using the Lorentz–Berthelot mixing rules. In the case of CO_2, partial point charges were located at the LJ centers: $q_O=-0.288$e and $q_C=0.576$e. Note that the calculation method was validated by comparing experimentally obtained isotherms (N_2 at 77 K and H_2 at 77 and 303 K) with the corresponding simulated isotherms on the pristine ZTC.

Acknowledgements

This research was partially supported by a NEDO Program, Advanced Fundamental Research on Hydrogen Storage Materials (Hydro-Star) (T.K.); by the Ministry of Education, Culture, Sports, Science and Technology, Grant-in-Aid for Scientific Research on the Innovative Areas: "Fusion Materials" (Area no. 2206), 23107507 (H.N.); and by the Cooperative Research Program of "Network Joint Research Center for Materials and Devices" (H.T.). H.T. thanks Dr. J. C. Palmer for fruitful discussions. We thank Japan EnviroChemicals, Ltd. for kindly supplying Shirasagi P.

[1] C. S. Cundy, P. A. Cox, *Microporous Mesoporous Mater.* **2005**, *82*, 1–78.
[2] M. E. Davis, R. F. Lobo, *Chem. Mater.* **1992**, *4*, 756–768.
[3] Y. S. Tao, H. Kanoh, L. Abrams, K. Kaneko, *Chem. Rev.* **2006**, *106*, 896–910.
[4] M. E. Davis, *Nature* **2002**, *417*, 813–821.
[5] C. T. Kresge, M. E. Leonowicz, W. J. Roth, J. C. Vartuli, J. S. Beck, *Nature* **1992**, *359*, 710–712.
[6] D. Y. Zhao, J. L. Feng, Q. S. Huo, N. Melosh, G. H. Fredrickson, B. F. Chmelka, G. D. Stucky, *Science* **1998**, *279*, 548–552.
[7] S. Kitagawa, R. Kitaura, S. Noro, *Angew. Chem.* **2004**, *116*, 2388–2430; *Angew. Chem. Int. Ed.* **2004**, *43*, 2334–2375.
[8] H. Li, M. Eddaoudi, M. O'Keeffe, O. M. Yaghi, *Nature* **1999**, *402*, 276–279.
[9] K. M. Thomas, *Dalton Trans.* **2009**, 1487–1505.
[10] S. A. Al-Muhtaseb, J. A. Ritter, *Adv. Mater.* **2003**, *15*, 101–114.
[11] J. Chmiola, G. Yushin, Y. Gogotsi, C. Portet, P. Simon, P. L. Taberna, *Science* **2006**, *313*, 1760–1763.
[12] J. Lee, J. Kim, T. Hyeon, *Adv. Mater.* **2006**, *18*, 2073–2094.
[13] R. Ryoo, S. H. Joo, M. Kruk, M. Jaroniec, *Adv. Mater.* **2001**, *13*, 677–681.
[14] H. Nishihara, T. Kyotani, *Adv. Mater.* **2012**, *24*, 4473–4498.
[15] P. D. Yang, T. Deng, D. Y. Zhao, P. Y. Feng, D. Pine, B. F. Chmelka, G. M. Whitesides, G. D. Stucky, *Science* **1998**, *282*, 2244–2246.
[16] B. T. Holland, C. F. Blanford, T. Do, A. Stein, *Chem. Mater.* **1999**, *11*, 795–805.
[17] T. Masuda, N. Fukumoto, M. Kitamura, S. R. Mukai, K. Hashimoto, T. Tanaka, T. Funabiki, *Microporous Mesoporous Mater.* **2001**, *48*, 239–245.
[18] H. Nishihara, Y. Fukuraa, K. Inde, K. Tsuji, M. Takeuchi, T. Kyotani, *Carbon* **2008**, *46*, 48–53.
[19] T. Kyotani, *Carbon* **2000**, *38*, 269–286.
[20] J. W. Diggle, T. C. Downie, C. W. Goulding, *Chem. Rev.* **1969**, *69*, 365–405.
[21] G. Alberti, S. Murcia-Mascaros, R. Vivani, *J. Am. Chem. Soc.* **1998**, *120*, 9291–9295.
[22] L. Carlucci, G. Ciani, M. Moret, D. M. Proserpio, S. Rizzato, *Angew. Chem.* **2000**, *112*, 1566–1570; *Angew. Chem. Int. Ed.* **2000**, *39*, 1506–1510.
[23] C. J. Kepert, T. J. Prior, M. J. Rosseinsky, *J. Am. Chem. Soc.* **2000**, *122*, 5158–5168.
[24] L. C. Tabares, J. A. R. Navarro, J. M. Salas, *J. Am. Chem. Soc.* **2001**, *123*, 383–387.
[25] J. Weber, M. Antonietti, A. Thomas, *Macromolecules* **2008**, *41*, 2880–2885.
[26] K. Kamegawa, H. Yoshida, *Carbon* **1997**, *35*, 631–639.
[27] K. Kaneko, *J. Membr. Sci.* **1994**, *96*, 59–89.
[28] J. J. Wu, X. Y. Liu, S. H. Tolbert, *J. Phys. Chem. B* **2000**, *104*, 11837–11841.
[29] T. A. Ezquerra, M. Garcia-Gutierrez, A. Nogales, M. Gomez, *Applications of Synchrotron Light to Scattering and Diffraction in Materials and Life Sciences*, Springer, Berlin, **2009**.
[30] Z. X. Ma, T. Kyotani, A. Tomita, *Chem. Commun.* **2000**, 2365–2366.
[31] H. Nishihara, Q. H. Yang, P. X. Hou, M. Unno, S. Yamauchi, R. Saito, J. I. Paredes, A. Martinez-Alonso, J. M. D. Tascon, Y. Sato, M. Terauchi, T. Kyotani, *Carbon* **2009**, *47*, 1220–1230.
[32] P. X. Hou, H. Orikasa, H. Itoi, H. Nishihara, T. Kyotani, *Carbon* **2007**, *45*, 2011–2016.
[33] K. W. Chapman, G. J. Halder, P. J. Chupas, *J. Am. Chem. Soc.* **2009**, *131*, 17546–17547.
[34] I. Beurroies, M. Boulhout, P. L. Llewellyn, B. Kuchta, G. Ferey, C. Serre, R. Denoyel, *Angew. Chem.* **2010**, *122*, 7688–7691; *Angew. Chem. Int. Ed.* **2010**, *49*, 7526–7529.
[35] H. Nishihara, P. X. Hou, L. X. Li, M. Ito, M. Uchiyama, T. Kaburagi, A. Ikura, J. Katamura, T. Kawarada, K. Mizuuchi, T. Kyotani, *J. Phys. Chem. C* **2009**, *113*, 3189–3196.
[36] K. S. Park, Z. Ni, A. P. Cote, J. Y. Choi, R. D. Huang, F. J. Uribe-Romo, H. K. Chae, M. O'Keeffe, O. M. Yaghi, *Proc. Natl. Acad. Sci. USA* **2006**, *103*, 10186–10191.
[37] J. C. Tan, B. Civalleri, C. C. Lin, L. Valenzano, R. Galvelis, P. F. Chen, T. D. Bennett, C. Mellot-Draznieks, C. M. Zicovich-Wilson, A. K. Cheetham, *Phys. Rev. Lett.* **2012**, *108*, 095502.
[38] M. Colligan, P. M. Forster, A. K. Cheetham, Y. Lee, T. Vogt, J. A. Hriljac, *J. Am. Chem. Soc.* **2004**, *126*, 12015–12022.
[39] P. H. Mott, J. R. Dorgan, C. M. Roland, *J. Sound Vib.* **2008**, *312*, 572–575.
[40] M. R. Falvo, G. J. Clary, R. M. Taylor, V. Chi, F. P. Brooks, S. Washburn, R. Superfine, *Nature* **1997**, *389*, 582–584.
[41] G. Eda, G. Fanchini, M. Chhowalla, *Nat. Nanotechnol.* **2008**, *3*, 270–274.
[42] C. Lee, X. D. Wei, J. W. Kysar, J. Hone, *Science* **2008**, *321*, 385–388.
[43] D. W. Breck, *Zeolite Molecular Sieves: Structure, Chemistry, and Use*, Wiley, New York, **1974**.
[44] Y. F. Shi, *J. Chem. Phys.* **2008**, *128*, 234707.
[45] J. C. Palmer, J. D. Moore, J. K. Brennan, K. E. Gubbins, *Adsorption* **2011**, *17*, 189–199.
[46] J. C. Palmer, J. D. Moore, T. J. Roussel, J. K. Brennan, K. E. Gubbins, *Phys. Chem. Chem. Phys.* **2011**, *13*, 3985–3996.
[47] R. Dawson, A. I. Cooper, D. J. Adams, *Prog. Polym. Sci.* **2012**, *37*, 530–563.

Received: May 11, 2013
Published online: August 28, 2013

